PCCP

ROYAL SOCIETY OF CHEMISTRY

PAPER

View Article Online
View Journal | View Issue

Cite this: *Phys. Chem. Chem. Phys.*, 2024, **26**, 477

Halogen bond catalysis of the [4+2] cycloaddition reaction of 2-alkenylindoles: catalytic modes and stereoselectivity†

Ying Li, Chang Zhao, Huaiyu Zhang* and Yanli Zeng *

Halogen bond donor catalysts have been widely used in organic reactions because they are environmentally friendly, inexpensive and recyclable. The [4+2] cycloaddition reaction is a key reaction in organic synthesis because of its ease of use, fast speed, and wide range of applications. In this work, halogen bond catalysis in the [4+2] cycloaddition reaction between 2-alkenylindoles was investigated based on DFT calculations. There are two modes of I···π halogen bond catalysis: either on the ethenyl of 2-alkenylindole (mode A) or on the five-membered ring of 2-alkenylindole (mode B). Both modes involve two steps: the formation of carbon–carbon bonds and the formation of six-membered rings. Gibbs free energy barriers were determined to investigate the stereoselectivity of the *endo* pathway and *exo* pathway. For mode A, the *exo* products were more easily generated when the substituent R = H, and the N–H···π interaction promoted high *endo* selectivity in the case of the substituent R = Ph. For mode B, an increasing proportion of *endo* products can be obtained in the order of catalyst I_2, IBr and ICl. The π···π interaction of the substituent R = Ph promotes the [4+2] cycloaddition reaction, which is consistent with the experimental observation that R = Ph has a higher yield than R = H. The study of different catalytic modes and stereoselectivity would provide new ideas for the further study of the [4+2] cycloaddition reaction.

Received 11th November 2023,
Accepted 4th December 2023

DOI: 10.1039/d3cp05479a

rsc.li/pccp

1. Introduction

Halogen bonds have been continuously developed in most chemical fields, from molecular recognition or drug design to supramolecular chemistry, materials science and catalytic chemistry.[1] Halogen bonds[2] are important noncovalent interactions that play an important role in catalysis, not only by controlling the reactivity of the conversion process but also by controlling selectivity to a considerable extent.[3]

Halogen bond donor catalysts, as environmentally friendly and recyclable reagents, have been widely used in organic reactions in recent years.[4,5] In 2008, Bolm *et al.*[6] reported the Hantzsch ester reduction of 2-phenylquinoline activated by halogen bonds, which is the application of halogen bonds in catalytic reactions. In the following years, halogen bond donors have been used as catalysts in different reactions by activating various functional groups, such as amides,[7,8] carbonyl groups,[9–11] halides,[12–14] nitro groups,[15] and imines.[16,17] In these reactions, halogen bond donor catalysts are mainly used to activate substrates containing lone pair-possessing heteroatoms to complete the catalytic reaction. However, there are fewer studies on halogen bond catalysis by activating the π-electrons of reactants in the [4+2] cycloaddition reaction.

The [4+2] cycloaddition reaction is a key reaction in organic synthesis because of its simple reaction, fast speed, wide range of application and mild reaction conditions. In 2019, Arai *et al.* first studied C–I···π halogen bond catalysis in the [4+2] cycloaddition reaction of 2-alkenylindoles by a cationic halogen bond donor catalyst.[18] Subsequently, they used hypervalent cyclic dibenzoiodolium salts as halogen bond donors to catalyse the [4+2] cycloaddition reaction and obtained a high yield.[19] Fernández *et al.* provided a detailed exploration of the nature of C–I···π halogen bonds and their role in organic catalysis using density functional theory (DFT) calculations.[20]

Dihalide molecules (I_2, IBr, ICl) as neutral halogen bond donor catalysts have been widely investigated in cyclization reactions. I_2 has been used as a catalyst and has shown good catalytic activity in [4+2] cycloaddition reactions.[21,22] IBr has excellent diastereoselectivity in the low-temperature electrophilic cyclization of homallyl carbonates.[23] ICl is generally easier to handle as a commercially available solution (1 M of dichloromethane/acetic acid), promoting its safe usage.[24] Chimni *et al.*

College of Chemistry and Materials Science, Hebei Normal University, Shijiazhuang, 050024, China. E-mail: yanlizeng@hebtu.edu.cn, huaiyu.zhang@hetu.edu.cn

† Electronic supplementary information (ESI) available: The I···C5 and I···C6 distances (in Å) in COM1a-*endo* catalysed by I_2, IBr, and ICl; the I···C5 and I···C6 distances (in Å) in COM1a-*exo* catalysed by I_2, IBr, and ICl; calculated Gibbs free energy and XYZ coordinates. See DOI: https://doi.org/10.1039/d3cp05479a

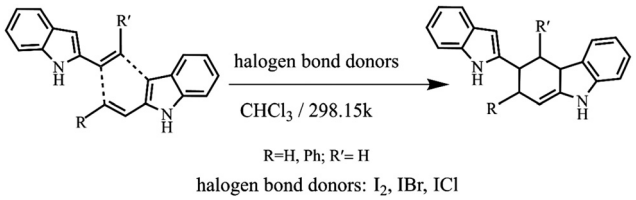

Scheme 1 The [4+2] cycloaddition reaction between the 2-alkenylindoles catalysed by halogen bond donors (I_2, IBr, ICl).

summarized the use of ICl for different types of cyclization reactions.[25] Therefore, neutral halogen bond donor catalysts (I_2, IBr, ICl) are expected to be studied for C–I···π halogen bond catalysis in the [4+2] cycloaddition reaction.

The [4+2] cycloaddition reaction is usually a one-step cyclization synergistic reaction, and the synergistic mechanism is not absolute, so there are great challenges in the research and control of the stepwise [4+2] cycloaddition reaction. It has been proven experimentally that stepwise cyclization can complete the [4+2] cycloaddition reaction (Diels–Alder reaction),[26] but whether the halogen bond-catalysed [4+2] cycloaddition reaction can achieve the stepwise reaction mechanism is worthy of further study.

In this work, neutral halogen bond donors (I_2, IBr, ICl) were used as catalysts, and the [4+2] cycloaddition reaction between the 2-alkenylindoles was investigated (Scheme 1). We will focus on the following points: (1) to explore the I···π halogen bond catalytic mechanism of the [4+2] cycloaddition reaction; (2) to search the I···π halogen bond catalytic modes of the [4+2] cycloaddition reaction; (3) to compare the stereoselectivity of the *endo* pathway and *exo* pathway; and (4) to give some insight into the relationship of the catalytic activity, catalytic modes, and stereoselectivity. Our study provides the basis for the selection of the catalytic mode and the control of stereoselectivity.

2. Computational details

Density functional theory (DFT) calculations based on the M06-2X functional[27] were performed using the Gaussian 16 package.[28] The M06-2X functional was chosen because it provides a good explanation of halogen bonds[29] and kinetics.[30–32] The 6-311G** base set[33] was used for C, H, N, and Cl atoms, and the aug-cc-pVTZ-PP basis set was used for Br and I atoms.[34] The solvent effect in trichloromethane ($CHCl_3$) was simulated by using the PCM implicit solvation model.[35,36] The frequency of each optimized stationary point was calculated at the same theoretical level to verify the local minima point and transition state. The local minima points and transition states have zero and one imaginary frequency, respectively. In addition, it is confirmed by the intrinsic reaction coordinates (IRCs)[37,38] that the transition state indeed connects the two related minima along the reaction path. To determine the effect of entropy on Gibbs free energy, the translation entropy correction of the solution was obtained by using Fang's THERMO program.[39]

The electrostatic potential (ESP)[40,41] was computed at the same level of theory and represented on the 0.001 a.u. electron density isosurface.[42] The ESP and independent gradient model based on Hirshfeld partition (IGMH) were calculated with the Multiwfn program (version 3.8)[43] and visualized by the VMD program.[44] The 3D structure of the studied species was displayed by CYLview software.[45]

3. Results and discussion

3.1 The uncatalysed [4+2] cycloaddition reaction pathway between 2-vinylindoles

Fig. 1 shows the calculated Gibbs free energy curves of the uncatalysed [4+2] cycloaddition reaction of 2-vinylindoles, with the black and red lines denoting the *endo* and *exo* pathways, respectively. The total energies of the 2-vinylindoles are set to zero, and all the energies of the stationary points are relative to zero.

For both the *endo* and *exo* pathways, when two 2-vinylindoles are close to each other, the complexes COM1-*endo* and COM1-*exo* are formed. Then, the C6 atom attacks the C1 atom, the C4 atom approaches the C5 atom, and products 1-*endo* and 1-*exo* are generated through TS1-*endo* and TS1-*exo*. The [4+2] cycloaddition reaction between the 2-vinylindoles involves a concerted mechanism, and the Gibbs free energy barriers (ΔG) of the *endo* and *exo* pathways were calculated to be 32.0 and 30.4 kcal mol^{-1}, respectively. The Gibbs free energy barriers of TS1-*endo* and TS1-*exo* are high, which indicates that the [4+2] cycloaddition reaction is difficult to proceed without catalysts.

3.2 The mechanism of the I···π halogen bond catalytic [4+2] cycloaddition reaction between 2-vinylindoles

Halogen bond donors (I_2, IBr, ICl) were used as catalysts to investigate the I···π halogen bond catalysis on the [4+2] cycloaddition reaction between 2-vinylindoles.

Electrostatic potential (ESP) calculations for 2-vinylindole and halogen bond donors were performed, as shown in Fig. 2. A halogen atom X (X = Cl, Br, I) in a molecule is usually negatively charged. However, the anisotropic distribution of its electron

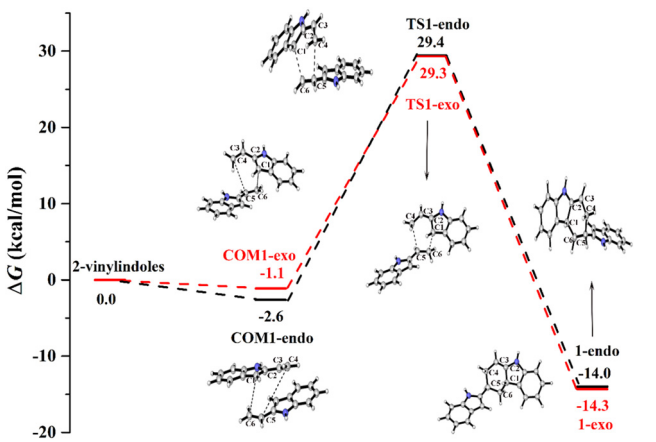

Fig. 1 Gibbs free energy curves of the uncatalysed [4+2] cycloaddition reaction between 2-vinylindoles.

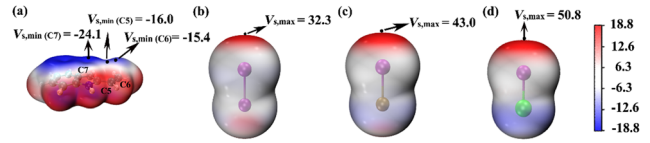

Fig. 2 Electrostatic potential maps on the 0.001 a.u. (electrons per bohr^3) contour of the electronic density (kcal mol^{-1}): (a) 2-vinylindole; (b) I_2; (c) IBr; (d) ICl.

density can lead to an electron-depleted σ-hole at the pole on the extension of the R–X bond and an electron-rich equatorial belt perpendicular to the bond direction.[46] The halogen bond can be understood as the attraction between the σ-hole and the negative site of another molecule.[47–49] For 2-vinylindole, the most negative values ($V_{s,min}$) exist outside the C5 and C6 atoms of ethenyl and the C7 atom of the five-membered ring, with $V_{s,min}$ values of −16.0, −15.4 and −24.1 kcal mol^{-1}, respectively. For I_2, IBr, and ICl, the most positive values ($V_{s,max}$) outside the I atom along the I–X (X = I, Br, Cl) bond axis are 32.3, 43.0, and 50.8 kcal mol^{-1}, respectively, increasing in the order of I_2, IBr and ICl. Therefore, it could be predicted that I···π halogen bonds could be formed *via* either C5═C6 of ethenyl or *via* the C7 atom of the five-membered ring.

Fig. 3 depicts the ESP surfaces of COM1a-*endo*, COM1a-*exo*, COM1b-*endo* and COM1b-*exo*. The van der Waals surface penetration can be clearly observed between the ethenyl of 2-vinylindoles and catalyst ICl, as well as between the five-membered ring of 2-vinylindoles and catalyst ICl. Red and blue regions penetrate each other, reflecting the complementary characteristics of electrostatic potentials, verifying that the ethenyl and five-membered rings of 2-vinylindoles can form halogen bonds with the catalyst ICl, respectively.

Fig. 4 shows the two catalytic modes of halogen bond activation to π electrons of the reactant. Mode A: The electrophilic catalysis of the I···π halogen bond between the catalyst and ethenyl of 2-vinylindoles; mode B: the electrophilic catalysis of the I···π halogen bond between the catalyst and the five-membered ring of 2-vinylindoles.

3.2.1 I···π halogen bond catalysis on the ethenyl of 2-vinylindoles. First, the [4+2] cycloaddition reaction catalysed by the I···π halogen bond between the catalysts (I_2, IBr, ICl) and the ethenyl of 2-vinylindoles was investigated. Taking the ICl catalyst as an example, the optimized geometries and key bond lengths along the IRC pathway of the [4+2] cycloaddition reaction are shown in Fig. 5.

When the catalyst attacks the ethenyl of 2-vinylindole, COM1a is formed. There are two stereo geometries in the *endo* and *exo* pathways, namely, COM1a-*endo* and COM1a-*exo*, respectively. From Tables S1 and S2 (ESI†), the distances of I···C5 and I···C6 in COM1a-*endo* and COM1a-*exo* are obviously shorter than the corresponding sum of van der Waals radii (3.68 Å) of I and C atoms, indicating that an I···π halogen bond is formed between the catalyst and ethenyl of 2-vinylindole. The I···C5 and I···C6 distances in COM1a-*endo* and COM1a-*exo* decrease along the sequence of I_2, IBr, and ICl, which are in accordance with the $V_{s,max}$ value of ESP. The larger the $V_{s,max}$ value of the halogen bond donor catalyst is, the shorter the I···π halogen bond distances and the stronger the halogen bond interaction.

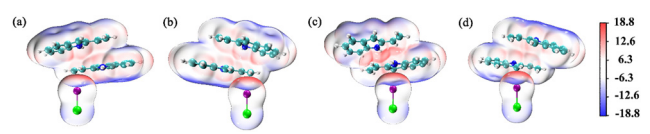

Fig. 3 Electrostatic potential maps on the 0.001 a.u. (electrons per bohr^3) contour of the electronic density (kcal mol^{-1}): (a) COM1a-*endo*, (b) COM1a-*exo*, (c) COM1b-*endo*, (d) COM1b-*exo*.

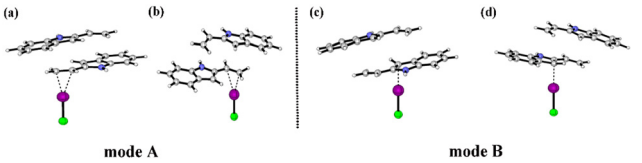

Fig. 4 Two modes of halogen bond activation to the reactant. Mode A: I···π halogen bond catalysis on the ethenyl of 2-vinylindoles; Mode B: I···π halogen bond catalysis on the five-membered ring of 2-vinylindoles. (a) COM1a-*endo*, (b) COM1a-*exo*, (c) COM1b-*endo*, (d) COM1b-*exo*.

With I···π halogen bond catalysis, the [4+2] cycloaddition reaction of 2-vinylindoles undergoes a stepwise mechanism, which is different from the concerted mechanism of the uncatalysed reaction. Both the *endo* and *exo* pathways involve two steps: the step of C1–C6 bond formation and the step of six-membered ring formation. The stepwise pathway of the I···π halogen bond catalytic [4+2] cycloaddition reaction in this work agrees with that of the electric field–catalysed single-molecule Diels–Alder reaction, which has been observed and confirmed in the experiment.[26]

For the *endo* pathway of the [4+2] cycloaddition reaction, Fig. 6 shows the Gibbs free energy curves of the *endo* pathway *via* I···π halogen bond catalysis on the ethenyl of 2-vinylindoles. Taking the catalyst ICl as an example, the catalytic processes were investigated. The catalytic reaction starts from COM1a-*endo* with a Gibbs free energy of −7.5 kcal mol^{-1}, and the distances of C1–C6, C4–C5, and C5–C6 are 3.726, 4.469 and 1.360 Å, respectively. After COM1a-*endo*, the C6 atom attacks the C1 atom, and the C5 atom approaches the C4 atom to form TS1a-*endo*. In TS1a-*endo*, the distances of C1–C6 and C4–C5 are 2.159 and 3.413 Å, respectively. After TS1a-*endo*, the C5–C6 distance is lengthened. When the C1–C6 distance reaches 1.570 Å, the C1–C6 bond is formed, and INT1a-*endo* is reached. The C1–C6 bond formation step occurs with a Gibbs free energy barrier (ΔG) of 17.1 kcal mol^{-1}. After INT1a-*endo*, the C4–C5 distance continues to be shortened to form a six-membered ring product 2a-*endo* *via* TS2a-*endo*. When the distances of C1–C6 and C4–C5 become 1.549 and 1.551 Å, the product 2a-*endo* is formed. The six-membered ring formation step is the rate-determining step, with a ΔG of 27.3 kcal mol^{-1} relative to INT1a-*endo*.

For the *exo* pathway of the [4+2] cycloaddition reaction, Fig. 7 shows the Gibbs energy curves of the *endo* pathway *via* I···π halogen bond catalysis on the ethenyl of 2-vinylindole.

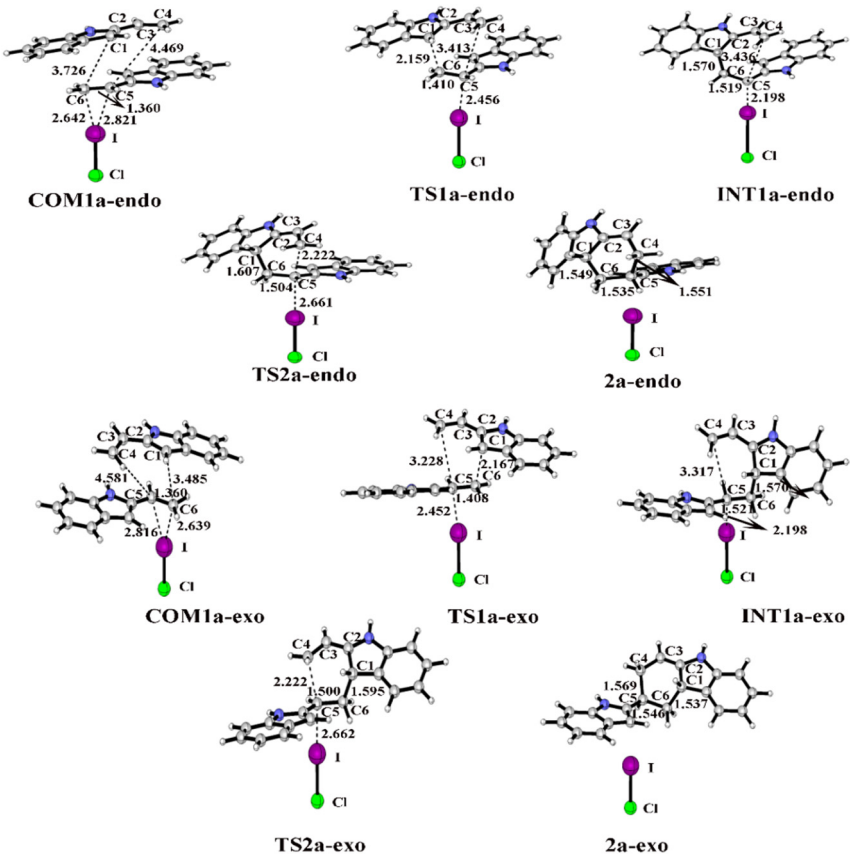

Fig. 5 Optimized geometries and key bond lengths (in Å) along the IRC pathway of I···π halogen bond catalysis *via* ICl activation on the ethenyl of 2-vinylindole.

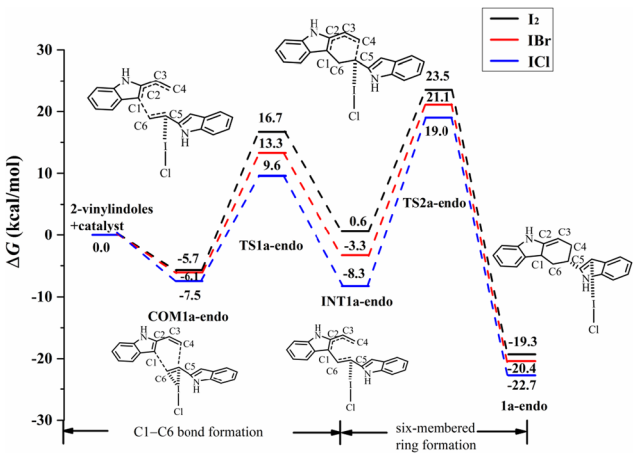

Fig. 6 Gibbs free energy curves of the *endo* pathway *via* I···π halogen bond catalysis on the ethenyl of 2-vinylindole (mode A).

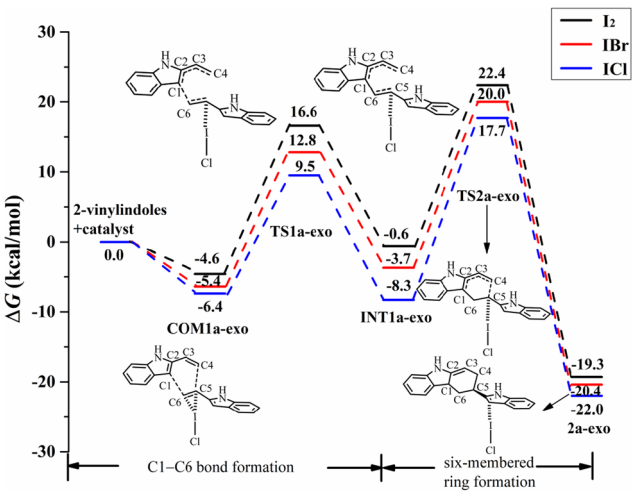

Fig. 7 Gibbs free energy curves of the *exo* pathway *via* I···π halogen bond catalysis on the ethenyl of 2-vinylindole (mode A).

The catalytic reaction starts from COM1a-*exo* with a Gibbs free energy of −6.4 kcal mol^{-1}, and the distances of C4–C5, C1–C6 and C5═C6 are 4.581, 3.485 and 1.360 Å, respectively. From COM1a-*exo* to INT1a-*exo*, the C1–C6 distance is shortened until the C1–C6 bond is formed. After INT1a-*exo*, the C4–C5 distance is constantly shortened, from 3.317 Å in INT1a-*exo* to 1.569 Å in 2a-*exo*. The Δ*G* values of the first step of C1–C6 bond formation and the second step of six-membered ring formation are 15.9 and 26.0 kcal mol^{-1}, respectively.

The catalysts I_2 and IBr also catalysed the [4+2] cycloaddition reaction by I···π halogen bonds. For I_2, IBr, and ICl, the Gibbs

free energies of COM1a-*endo* are −5.7, −6.1, and −7.5 kcal mol^{-1}, respectively, and those of COM1a-*exo* are −4.6, −5.4, and −6.4 kcal mol^{-1}, respectively, as shown in Fig. 6 and 7. According to the order of I_2, IBr and ICl, the exothermic heat of COM1a increases with the gradual strengthening of the halogen bond. For the *endo* pathway catalysed by I_2, IBr and ICl, the ΔG values needed for the formation of the C1–C6 bond are 22.4, 19.4, and 17.1 kcal mol^{-1}, and those needed for the formation of the six-membered ring are 29.2, 27.2, and 27.3 kcal mol^{-1}, respectively. For the *exo* pathway catalysed by I_2, IBr and ICl, the ΔG values of C1–C6 bond formation are 21.2, 18.2, and 15.9 kcal mol^{-1}, respectively, and those of six-membered ring formation are 27.0, 25.4, and 26.0 kcal mol^{-1}, respectively.

Comparing the ΔG values of the two steps, the formation of the six-membered ring is the rate-determining step for mode A. For the process of six-membered ring formation, the ΔG values of the *exo* pathway are somewhat lower than those of the *endo* pathway, indicating that the [4+2] cycloaddition reaction *via* I···π halogen bond catalysis on the ethenyl of 2-vinylindole can proceed smoothly, the *exo* pathway is preferred, and the product of the *exo* pathway is the main product. In the products of 2a-*endo* and 2a-*exo*, the interaction between the catalysts (I_2, IBr, ICl) and the substrate is a relatively weaker halogen bond than that of COM1a-*exo* and COM1a-*endo*, indicating that the catalysts (I_2, IBr, ICl) can be separated easily and then carry out the catalytic cycle.

3.2.2 I···π halogen bond catalysis on the five-membered ring of 2-vinylindole. The [4+2] cycloaddition reaction catalysed by the I···π halogen bond between the catalysts (I_2, IBr, ICl) and the five-membered ring of 2-vinylindole was investigated. The electrophilic catalytic mechanism of I···π halogen bond catalysis on the five-membered ring of 2-vinylindole: the formation of C1–C6 bond and the formation of six-membered ring.

For the *endo* pathway of the [4+2] cycloaddition reaction, the optimized geometries and key bond lengths along the IRC pathway of the [4+2] cycloaddition reaction are shown in Fig. 8. Taking the ICl catalyst as an example, the distances of C1···C6 and C4···C5 in COM1b-*endo* are 3.748 and 4.524 Å, respectively, and the C1···C6 distance is shorter than that of C4···C5, indicating that C1···C6 forms a bond before C4···C5. The C1···C6 distance gradually shortened from 3.748 Å in COM1b-*endo* to 1.595 Å in INT1b-*endo*, and a C1–C6 bond was formed in INT1b-*endo*.

For the *endo* pathway of the [4+2] cycloaddition reaction, Fig. 9 shows the Gibbs free energy curves *via* I···π halogen bond catalysis on the five-membered ring of 2-vinylindole. COM1b-*endo* undergoes C1–C6 bond formation *via* TS1b-*endo* to INT1b-*endo* with a ΔG value of 18.0 kcal mol^{-1} relative to COM1b-*endo*, and C1–C6 bond formation is the rate-determining step for the *endo* pathway. After INT1b-*endo*, the *endo* pathway is accompanied by a shortening of the C4–C5 distance from 3.099 Å in INT1b-*endo* to 1.568 Å in 2c-*endo*. As shown in Fig. 9, the ΔG value of six-membered ring formation is 15.5 kcal mol^{-1} relative to COM1b-*endo*.

For the *exo* pathway of the [4+2] cycloaddition reaction, Fig. 10 shows the Gibbs free energy curves *via* I···π halogen

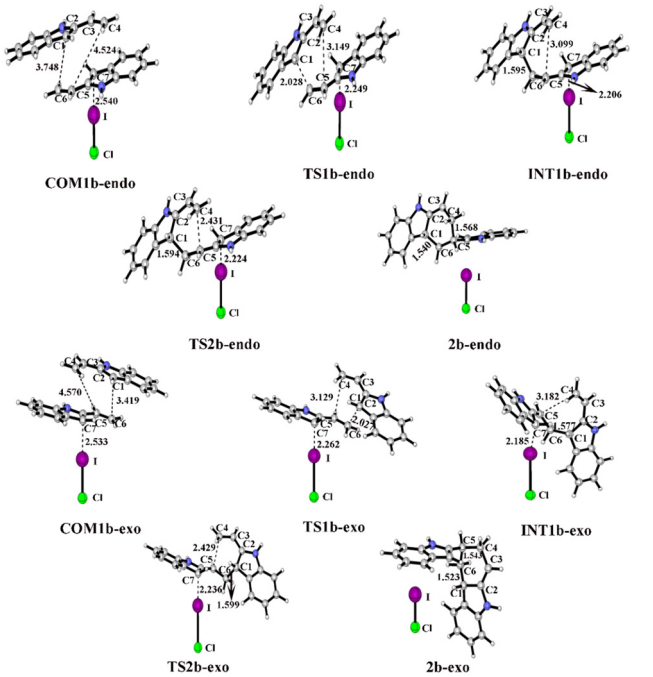

Fig. 8 Optimized geometries and key bond lengths (in Å) along the IRC pathway of I···π halogen bond catalysis *via* ICl activation on the five-membered ring of 2-vinylindole.

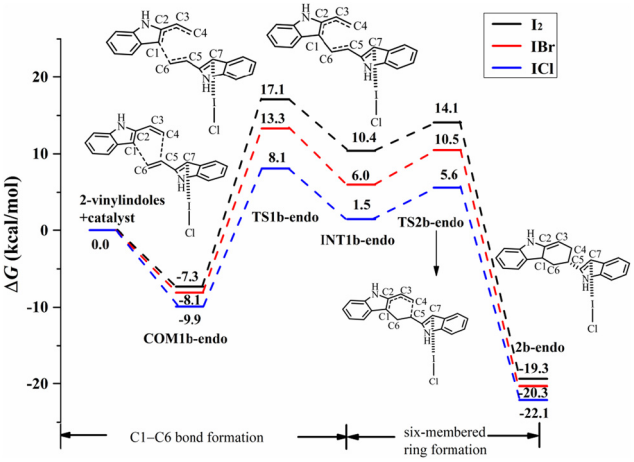

Fig. 9 Gibbs free energy curves of the *endo* pathway *via* I···π halogen bond catalysis on the five-membered ring of 2-vinylindole (mode B).

bond catalysis on the five-membered ring of 2-vinylindole. A stable complex is formed *via* 2-vinylindoles with halogen bond donor ICl, namely, COM1b-*exo*, and the Gibbs free energy is −9.9 kcal mol^{-1}. Then, INT1b-*exo* was formed by shortening the C1–C6 distance from 3.419 Å in COM1b-*exo* to 1.577 Å in INT1b-*exo via* TS1b-*exo*, which requires an energy barrier of 19.8 kcal mol^{-1}, and C1–C6 bond formation is the rate-determining step for the *exo* pathway. After INT1b-*exo*, the C4–C5 distance (3.182 Å) in INT1b-*exo* was noticeably shortened compared to that in 2b-*exo* (1.543 Å). The calculated ΔG value for this step is 17.4 kcal mol^{-1} relative to COM1b-*exo*.

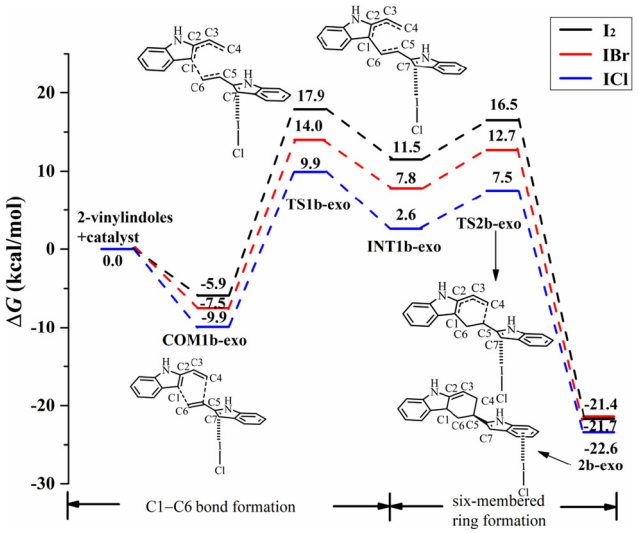

Fig. 10 Gibbs free energy curves of the *exo* pathway *via* I···π halogen bond catalysis on the five-membered ring of 2-vinylindole (mode B).

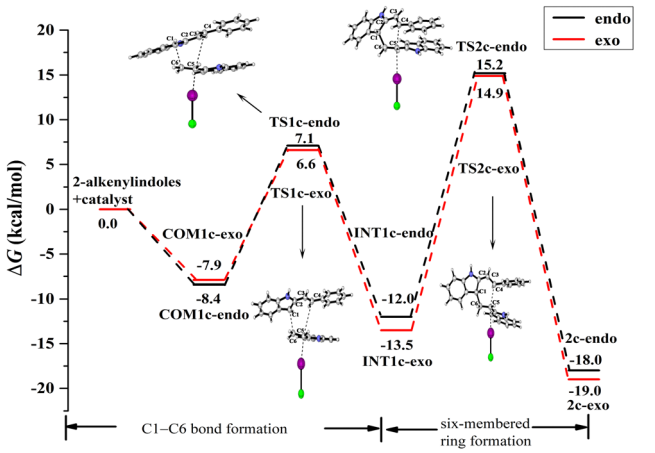

Fig. 11 ICl-catalysed Gibbs free energy curves of the *endo*- and *exo*-pathways *via* mode A for the reactant substituent R = Ph.

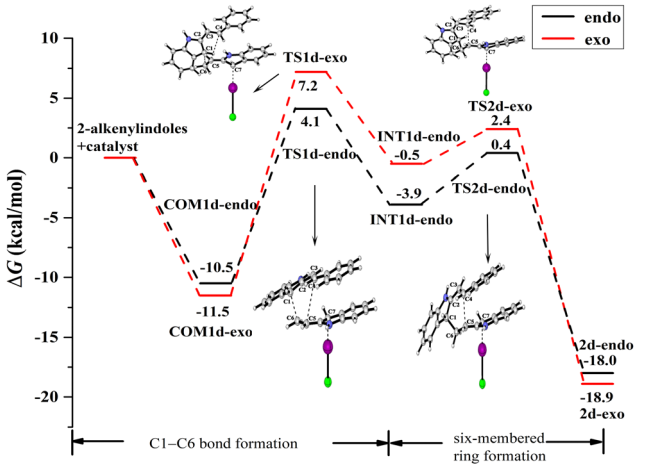

Fig. 12 Gibbs free energy curves of *endo* and *exo* pathways *via* mode B when the reactant substituent R = Ph.

The catalysts I_2 and IBr also catalysed the [4+2] cycloaddition reaction by I···π halogen bonds with the five-membered ring of 2-vinylindole, as shown in Fig. 9 and 10. The reaction mechanism is the same as that of ICl catalysis. The order of ΔG values of the halogen bond catalyst was I_2 > IBr > ICl, and the catalytic activity of the halogen bond donor catalyst increased in the order of I_2, IBr and ICl, which was consistent with the law of $V_{s,max}$ value of ESP.

Comparing the Gibbs free energy barriers of the two steps of mode B, the C1–C6 bond formation step has a higher Gibbs free energy barrier than the six-membered ring formation step, so the C1–C6 bond formation step is the rate-determining step. For the rate-determining step, the ΔG value of the *exo* pathway catalysed by I_2 is somewhat lower than that of the *endo* pathway, and the *endo* product can be obtained by I_2 catalysis. For IBr and ICl, the ΔG values of the *endo* pathway are lower than those of the *exo* pathway, and the *endo* products are easier to obtain. Therefore, an increasing proportion of *endo* products can be obtained in the order of catalyst I_2, IBr and ICl. It is further indicated that the catalytic activity of the catalyst has a certain effect on the stereoselectivity of the reaction. Different reaction products can be obtained by controlling the catalyst and different reaction modes.

3.2.3 Effects of substituents on the [4+2] cycloaddition reaction. To further investigate the influence of substituents on the [4+2] cycloaddition reaction, the substituents R = Ph and R′ = H for two reactant substrates were used in this section. Fig. 11 and 12 show the ICl-catalysed Gibbs free energy curves of mode A and mode B, respectively. For both modes, the reaction mechanism of substituent R = Ph is the same as that of R = H in Sections 3.2.1 and 3.2.2, including the formation of the C1–C6 bond and the six-membered ring.

For the *endo* pathway of mode A, the formation of the C1–C6 bond and the six-membered ring needs to overcome the ΔG of 15.5 kcal mol^{-1} and 27.2 kcal mol^{-1}, respectively. For the *exo* pathway of mode A, the formation of the C1–C6 bond and the six-membered ring needs to overcome the ΔG of 14.5 kcal mol^{-1} and 28.4 kcal mol^{-1}, respectively. For mode A, as shown in Fig. 13a and b, the N–H···π interaction exists between the two reaction substrates in COM1c-*endo* and INT1c-*endo* along the *endo* pathway, while the N–H···π interaction does not exist in COM1c-*exo* and INT1c-*exo* along the *exo* pathway. When the substituent R = H of mode A, the *exo* pathway is somewhat easier than the *endo* pathway. While for the substituent R = Ph of mode A, the N–H···π interaction makes the ΔG value of the *endo* pathway (27.2 kcal mol^{-1}) lower than that of the *exo* pathway (28.4 kcal mol^{-1}) at the rate-determining step. Therefore, the N–H···π interaction promotes high *endo* selectivity.

For the *endo* pathway of mode B, the formation of the C1–C6 bond and the six-membered ring formation needs to overcome the ΔG of 14.6 kcal mol^{-1} and 10.9 kcal mol^{-1}, respectively. For the *exo* pathway of mode B, the calculated ΔG values for C1–C6 bond formation and six-membered ring formation are 18.7 and

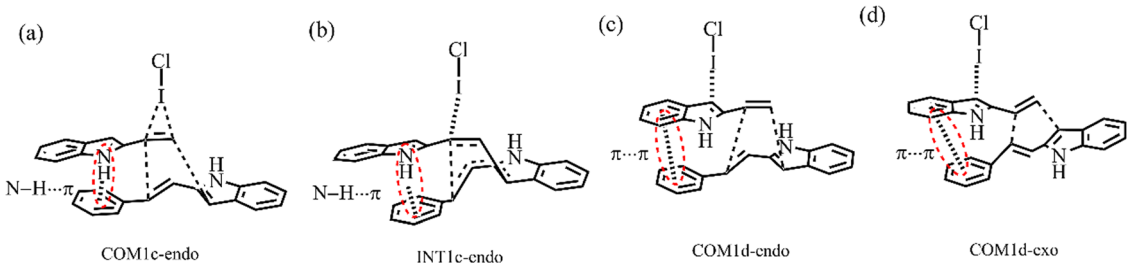

Fig. 13 Structures of COM1c-*endo*, INT1c-*endo*, COM1d-*endo*, COM1d-*exo*.

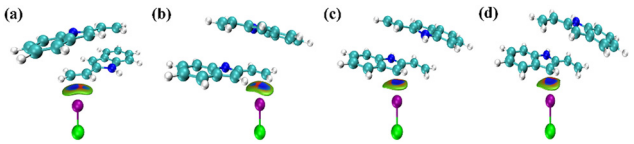

Fig. 14 IGMH coloring isosurface maps for the COM1a-*endo* (a), COM1a-*exo* (b), COM1b-*endo* (c) and COM1b-*exo* (d).

13.9 kcal mol^{-1}, respectively. The ΔG values of the *endo* pathway are lower than those of the *exo* pathway, the *endo* product is more easily generated for mode B, not only for the substituent is H but also Ph. When the substituent R = Ph, due to the π···π interaction between the two substrates in COM1d-*endo* and COM1d-*exo* (Fig. 13c and d), the ICl-catalysed ΔG values are significantly lower than R = H, which is consistent with the experimental observation that R = Ph has the higher yield than R = H.[18] For the substituent R = Ph, the π···π interaction promotes the [4+2] cycloaddition reaction.

3.3 IGMH analysis

IGMH can intuitively understand the interaction of chemical systems by analysing molecular and periodic systems, weak interactions and chemical bonds.[50,51] Fig. 14 shows the IGMH plot of the COM1a-*endo*, COM1a-*exo*, COM1b-*endo* and COM1b-*exo*. Blue isosurfaces exist between the ethenyl of 2-vinylindoles and ICl in COM1a-*endo* and COM1a-*exo*, also exist between the five-membered ring of 2-vinylindoles and ICl in COM1b-*endo* and COM1b-*exo*. The IGMH plot analysis proves the weak attractive property of the interaction. Therefore, halogen-bonded interactions exist between the ethenyl of 2-vinylindoles and ICl, also exist between the five-membered ring of 2-vinylindoles and ICl.

4. Conclusions

The halogen bond donor (I_2, IBr, ICl)-catalysed [4+2] cycloaddition reaction between the 2-alkenylindoles was investigated based on DFT calculations. The catalytic modes, mechanism, and stereoselectivity have been systematically discussed. For the uncatalysed reaction, both the *endo* pathway and *exo* pathway are carried out in a concerted mechanism, and it is difficult to proceed at room temperature because of the high energy barriers.

For the [4+2] cycloaddition reaction between 2-alkenylindoles, the catalytic process facilitated by halogen bond donors (I_2, IBr, ICl) includes two modes: mode A refers to the electrophilic catalysis of the I···π halogen bond formed between the catalyst and ethenyl of 2-alkenylindole; mode B refers to the catalyst attacking the five-membered ring of 2-alkenylindole. Both mode A and mode B are stepwise and involve two steps: the formation of carbon–carbon bonds and the formation of six-membered rings. The formation of the six-membered ring is the rate-determining step for mode A, and the formation of the carbon–carbon bond is the rate-determining step for mode B.

Both catalytic modes include the *exo* pathway and *endo* pathway. For mode A, when the substituent R = H, the *exo*-pathway is somewhat easier than the *endo*-pathway. For the substituent R = Ph, the N–H···π interaction makes the reaction barrier of the *endo*-pathway lower than that of the *exo*-pathway at the rate-determining step. The N–H···π interaction promotes the high *endo* selectivity of mode A. For mode B, an increasing proportion of *endo* products can be obtained in the order of catalyst I_2, IBr and ICl. For the substituent R = Ph, the π···π interaction results in lower reaction energies in both the *endo* and *exo* pathways compared with R = H at the rate-determining step, which is consistent with the experimental observation that R = Ph has a higher yield than R = H. Overall, different catalytic modes and stereoselectivities can expand the study of [4+2] cycloaddition reactions in the future.

Conflicts of interest

There are no conflicts to declare.

Acknowledgements

This work was funded by the Natural Science Foundation of Hebei Province (B2022205022), the Science Research Project of Hebei Education Department (ZD2022103), the Innovation Capability Improvement Plan Project of Hebei Province (22567604H) and Graduate Innovation Ability Cultivation Funding Project of Hebei Province (Grants No. CXZZBS2023089).

References

1 G. Cavallo, P. Metrangolo, R. Milani, T. Pilati, A. Priimagi, G. Resnati and G. Terraneo, *Chem. Rev.*, 2016, **116**, 2478–2601.

2 A. S. Mahadevi and G. N. Sastry, *Chem. Rev.*, 2016, **116**, 2775–2825.
3 K. T. Mahmudov, M. N. Kopylovich, M. F. C. Guedes da Silva and A. J. L. Pombeiro, *Noncovalent Interactions in Catalysis*, Royal Society of Chemistry, London, 2019.
4 A. E. Settle, L. Berstis, S. Zhang, N. A. Rorrer, H. Hu, R. M. Richards, G. T. Beckham, M. F. Crowley and D. R. Vardon, *ChemSusChem*, 2018, **11**, 1768–1780.
5 A. Yoshimura and V. V. Zhdankin, *Chem. Rev.*, 2016, **116**, 3328–3435.
6 C. Bolm, A. Bruckmann and M. Pena, *Synlett*, 2008, 900–902.
7 A. Matsuzawa, S. Takeuchi and K. Sugita, *Chem. – Asian J.*, 2016, **11**, 2863–2866.
8 V. Mamane, P. Peluso, E. Aubert, R. Weiss, E. Wenger, S. Cossu and P. Pale, *Organometallics*, 2020, **39**, 3936–3950.
9 S. Portela, J. J. Cabrera-Trujillo and I. Fernandez, *J. Org. Chem.*, 2021, **86**, 5317–5326.
10 H. Zhang and P. H. Toy, *Adv. Synth. Catal.*, 2020, **363**, 215–221.
11 X. Liu, S. Ma and P. H. Toy, *Org. Lett.*, 2019, **21**, 9212–9216.
12 Y. Wang and P. Su, *ACS Omega*, 2020, **5**, 21862–21872.
13 A. Dreger, E. Engelage, B. Mallick, P. D. Beer and S. M. Huber, *Chem. Commun.*, 2018, **54**, 4013–4016.
14 K. Takagi, K. Yamauchi and H. Murakata, *Chem. – Eur. J.*, 2017, **23**, 9495–9500.
15 N. Tarannam, M. H. H. Voelkel, S. M. Huber and S. Kozuch, *J. Org. Chem.*, 2022, **87**, 1661–1668.
16 C. Zhao, C. Sun, X. Li and Y. Zeng, *ChemistrySelect*, 2021, **6**, 12843–12851.
17 W. He, Y. C. Ge and C. H. Tan, *Org. Lett.*, 2014, **16**, 3244–3247.
18 S. Kuwano, T. Suzuki, M. Yamanaka, R. Tsutsumi and T. Arai, *Angew. Chem., Int. Ed.*, 2019, **58**, 10220–10224.
19 Y. Nishida, T. Suzuki, Y. Takagi, E. Amma, R. Tajima, S. Kuwano and T. Arai, *ChemPlusChem*, 2021, **86**, 741–744.
20 S. Portela and I. Fernández, *Eur. J. Org. Chem.*, 2021, 6102–6110.
21 P. Vermeeren, T. A. Hamlin, I. Fernandez and F. M. Bickelhaupt, *Angew. Chem., Int. Ed.*, 2020, **59**, 6201–6206.
22 S. P. Chavan, P. Sharma, G. Rama Krishna and M. Thakkar, *Tetrahedron Lett.*, 2003, **44**, 3001–3003.
23 J. J. Duan and A. B. Smith III, *J. Org. Chem.*, 1993, **58**, 3703–3711.
24 D. P. Day, N. I. Alsenani and A. A. Alsimaree, *Eur. J. Org. Chem.*, 2021, 4299–4307.
25 S. Chimni and S. Singh, *Synthesis*, 2015, 1961–1989.
26 C. Yang, Z. Liu, Y. Li, S. Zhou, C. Lu, Y. Guo, M. Ramirez, Q. Zhang, Y. Li, Z. Liu, K. N. Houk, D. Zhang and X. Guo, *Sci. Adv.*, 2021, **7**, eabf0689.
27 Y. Zhao and D. G. Truhlar, *Theor. Chem. Acc.*, 2007, **120**, 215–241.
28 M. J. Frisch, G. W. Trucks, H. B. Schlegel, G. E. Scuseria, M. A. Robb, J. R. Cheeseman, G. Scalmani, V. Barone, G. A. Petersson, H. Nakatsuji, X. Li, M. Caricato, A. V. Marenich, J. Bloino, B. G. Janesko, R. Gomperts, B. Mennucci, H. P. Hratchian, J. V. Ortiz, A. F. Izmaylov, J. L. Sonnenberg, D. Williams-Young, F. Ding, F. Lipparini, F. Egidi, J. Goings, B. Peng, A. Petrone, T. Henderson, D. Ranasinghe, V. G. Zakrzewski, J. Gao, N. Rega, G. Zheng, W. Liang, M. Hada, M. Ehara, K. Toyota, R. Fukuda, J. Hasegawa, M. Ishida, T. Nakajima, Y. Honda, O. Kitao, H. Nakai, T. Vreven, K. Throssell, J. A. Montgomery, Jr., J. E. Peralta, F. Ogliaro, M. J. Bearpark, J. J. Heyd, E. N. Brothers, K. N. Kudin, V. N. Staroverov, T. A. Keith, R. Kobayashi, J. Normand, K. Raghavachari, A. P. Rendell, J. C. Burant, S. S. Iyengar, J. Tomasi, M. Cossi, J. M. Millam, M. Klene, C. Adamo, R. Cammi, J. W. Ochterski, R. L. Martin, K. Morokuma, O. Farkas, J. B. Foresman and D. J. Fox, *Gaussian 16, Revision C.01*, Gaussian, Inc., Wallingford CT, 2019.
29 S. Kozuch and J. M. Martin, *J. Chem. Theory Comput.*, 2013, **9**, 1918–1931.
30 J. Y. See, H. Yang, Y. Zhao, M. W. Wong, Z. Ke and Y.-Y. Yeung, *ACS Catal.*, 2018, **8**, 850–858.
31 H. Yang and M. W. Wong, *J. Am. Chem. Soc.*, 2013, **135**, 5808–5818.
32 Y. Zhao and D. G. Truhlar, *Acc. Chem. Res.*, 2008, **41**, 157–167.
33 R. Krishnan, J. S. Binkley, R. Seeger and J. A. Pople, *J. Chem. Phys.*, 1980, **72**, 650–654.
34 K. L. Schuchardt, B. T. Didier, T. Elsethagen, L. Sun, V. Gurumoorthi, J. Chase, J. Li and T. L. Windus, *J. Chem. Inf. Model.*, 2007, **47**, 1045–1052.
35 J. Tomasi, B. Mennucci and R. Cammi, *Chem. Rev.*, 2005, **105**, 2999–3094.
36 E. Cancès and B. Mennucci, *J. Chem. Phys.*, 2001, **114**, 4744–4745.
37 K. Fukui, *Acc. Chem. Res.*, 1981, **14**, 363–368.
38 K. Ishida, K. Morokuma and A. Komornicki, *J. Chem. Phys.*, 1977, **66**, 2153–2156.
39 D. C. Fang, *THERMO*, Beijing Normal University, Beijing, China, 2013.
40 J. Zhang and T. Lu, *Phys. Chem. Chem. Phys.*, 2021, **23**, 20323–20328.
41 T. Lu and F. Chen, *J. Mol. Graphics Modell.*, 2012, **38**, 314–323.
42 J. S. Murray, P. Lane and P. Politzer, *Int. J. Quantum Chem.*, 2007, **107**, 2286–2292.
43 T. Lu and F. Chen, *J. Comput. Chem.*, 2012, **33**, 580–592.
44 W. Humphrey, A. Dalke and K. Schulten, *J. Mol. Model.*, 1996, **14**, 33–38.
45 C. Y. Legault, *CYLview 20*, Université de Sherbrooke, 2020, **https://www.cylview.org**.
46 T. Clark, M. Hennemann, J. S. Murray and P. Politzer, *J. Mol. Model.*, 2007, **13**, 291–296.
47 P. Politzer, J. S. Murray and T. Clark, *Phys. Chem. Chem. Phys.*, 2010, **12**, 7748–7757.
48 P. Politzer, J. S. Murray and T. Clark, *Phys. Chem. Chem. Phys.*, 2013, **15**, 11178–11189.
49 P. Politzer, J. S. Murray, T. Clark and G. Resnati, *Phys. Chem. Chem. Phys.*, 2017, **19**, 32166–32178.
50 A. V. Rozhkov, E. A. Katlenok, M. V. Zhmykhova, A. Y. Ivanov, M. L. Kuznetsov, N. A. Bokach and V. Y. Kukushkin, *J. Am. Chem. Soc.*, 2021, **143**, 15701–15710.
51 T. Lu and Q. Chen, *Comprehensive Computational Chemistry*, 2024, vol. 2, pp. 240–264.

